Article

Side Chain Disorder and Phase Transitions in Alkyl-Substituted, Conjugated Oligomers. Relation to Side-Chain Melting in P3ATs

M. David Curtis, John I. Nanos, Hyunsik Moon, and Woong Sang Jahng

J. Am. Chem. Soc., **2007**, 129 (48), 15072-15084 • DOI: 10.1021/ja076235t

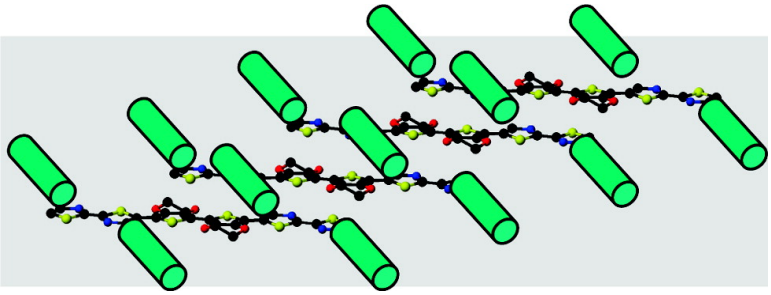

J|A|C|S
ARTICLES
Published on Web 11/08/2007

Side Chain Disorder and Phase Transitions in Alkyl-Substituted, Conjugated Oligomers. Relation to Side-Chain Melting in P3ATs

M. David Curtis,* John I. Nanos, Hyunsik Moon, and Woong Sang Jahng

Contribution from the Department of Chemistry and the Macromolecular Science and Engineering Program, The University of Michigan, Ann Arbor, Michigan 48109

Received August 18, 2007; E-mail: mdcurtis@umich.edu

Abstract: Certain 4,4′-alkyl substituted 2,2′-bithiazole and bithiazole-thiophene oligomers display an endothermic transition in their DSC trace below their respective melting points. Variable-temperature FTIR, MAS-^{1}H NMR, UV−vis spectra, and XRD all indicate that the thermal transition is due to a crystal−crystal phase transition that we have labeled $\alpha \rightarrow \beta$. FTIR shows a stepwise increase in the concentration of gauche defects at the $\alpha \rightarrow \beta$ transition temperature, but MAS NMR spectra show little increase in the side chain motion until the mp is reached. UV−vis spectra demonstrate that the conjugated main chains remain essentially planar through the $\alpha \rightarrow \beta$ transition, and significant deviations from planarity occur only at higher temperatures, but well below the mp. The close similarity of this behavior to the phase transitions in long chain *n*-paraffins and the "side-chain melting" phenomenon in poly(3-alkylthiophenes), P3ATs, suggests that the latter may actually be more accurately described as a crystal−crystal phase transition of the crystalline fraction, driven by side chain disorder.

Introduction

Applications, e.g., RF tags (smart and passive), large-area, flat-panel displays,[1] OFETs,[2] OLEDs,[3,4] sensors,[5] batteries,[6] nonlinear optics,[7] solar cells, and photovoltaic cells,[8] continue to push interest in the properties of conjugated materials.[9] Widely studied conjugated materials include, inter alia, oligo- and poly thiophenes,[10,11] pentacene derivatives,[12] and thieno-thiophenes.[13] Bithiazole oligomers and polymers are an interesting compliment to these classes of compounds. Thiophenes and pentacenes are relatively electron rich, are p-dopable, and are primarily p-type semiconductors. In contrast, bithiazoles are electron deficient and *n*-dopable.[14,15]

In certain applications, e.g., OFETs, batteries, and solar cells, high charge mobility is necessary. Charge mobility is intimately connected to the solid-state structure either via the conduction- or valence-bandwidth (coherent transport), or via the transfer integral and reorganization energy (hopping transport).[16] The molecular organization in a solid has a strong influence on the magnitudes of the bandwidth and transfer integral. Both quantities are enhanced by a regular, crystalline structure in which there are close intermolecular contacts.[17]

(1) (a) Dimitrakopoulos, C. D.; Malenfant, P. R. L. *Adv. Mater*. **2002**, *14*, 99. (b) Sun, Y.; Liu, Y.; Zhu, D. *J. Mater. Chem.* **2005**, *15*, 53.
(2) (a) Bao, Z. N. *Adv. Mater*. **2000**, *12*, 227. (b) Katz, H. E. *J. Mater. Chem.* **1997**, *7*, 369−376.
(3) (a) Sirringhaus, H.; Tessler, N.; Friend, R. H. *Synth. Met.* **1999**, *102*, 857−860. (b) Ho, P. K. H.; Tessler, N.; Friend, R. H. *Synth. Met.* **1999**, *102*, 1020−1020.
(4) Ho, P. K. H.; Thomas, D. S.; Friend, R. H.; Tessler, N. *Science* **1999**, *285*, 233−236; Friend, R.; Burroughes, J.; Shimoda, T. *Phys. World* **1999**, *12*, 35−40.
(5) Osada, Y. *Polymer Sensors and Actuators*; Springer-Verlag: New York, 1999.
(6) Genies, E. M.; Hany, P.; Santier, C. J. *Appl. Electrochem.* **1988**, *18*, 751−756.
(7) Tessler, N.; Pinner, D. J.; Cleave, V.; Ho, P. K. H.; Friend, R. H.; Yahioglu, G.; Barny, P. L.; Gray, J.; de Souza, M.; Rumbles, G. *Synth. Met.* **2000**, *115*, 57−62.
(8) (a) Brabec, C. J.; Cravino, A.; Meissner, D.; Sariciftci, N. S.; Fromherz, T.; Rispens, M. T.; Sanchez, L.; Hummelen, J. C. *Adv. Funct. Mater*. **2001**, *11*, 374−380. (b) Yu, G.; Wang, J.; McElvain, J.; Heeger, A. J. *Adv. Mater*. **1998**, *10*, 1431−1434. (c) Spanggaard, H.; Krebs, F. C. *Sol. Energy Mater. Sol. Cells* **2004**, *83*, 125−146.
(9) Forrest, S. R., Thompson, M. E., guest Eds. *Chem. Rev*. **2007**, *107*, Issue 4, is devoted to reviews of many aspects of organic electronics, including applications and theory.
(10) Otsubo, T.; Aso, Y.; Takimiya, *K. J. Mater. Chem.* **2002**, *12*, 2565 − 2575.
(11) (a) Jaiswal, M.; Menon, R. *Polym. Int.* **2006**, *55*, 1371−1384.
(12) (a) Anthony, J. *Chem. Rev.* **2006** *106*, 5028−5048, (b) Moon, H.; Zeis, R.; Borkent, E.-J.; Besnard, C.; Lovinger, A. J.; Siegrist, T.; Kloc, C.; Bao, Z. *J. Am. Chem. Soc.* **2004**, *126*, 15322.
(13) (a) Osuna, R. M.; Zhang, X.; Matzger, A. J.; Hernandez, V.; Lopez-Navarrete, J. T. *J. Phys. Chem. A.* **2006**, *15*, 5058−5065. (b) Zhang, X.; Johnson, J. P.; Kampf, J. W.; Matzger, A. J. *Chem. Mater*. **2006**, *18*, 3470−3476.
(13) (a) Nanos, J. I.; Kampf, J. W.; Curtis, M. D. *Chem. Mater*. **1995**, *7*, 2232−2234. (b) Politis, J. K.; Somoza, F. B., Jr.; Kampf, J. W.; Curtis, M. D.; Gonzalez Ronda, L.; Martin, D. C. *Chem. Mater*. **1999**, *11*, 2274−2284. (c) Curtis, M. D.; Cheng, H.-T.; Nanos, J. I.; Nazri, G.-A. *Macromolecules* **1998**, *31*, 205. (d) Politis, J. K.; Curtis, M. D.; Gonzalez Ronda, L.; Martin, D. C.; He, Y.; Kanicki, J. *Chem. Mater*. **1998**, *10*, 1713−1719.
(14) (a) Yamamoto, T.; Suganuma, H.; Maruyama, T.; Inoue, T.; Muramatsu, Y.; Arai, .; Komarudin, D.; Ooba, N.; Tomaru, S.; Sasaki, S.; Kubota, K. *Chem. Mater*. **1997**, *9*, 1217 −1225. (b) Yamamoto, T.; Maruyama, T.; Suganuma, H.; Arai, M.; Komarudin, D.; Sasaki S. *Chem. Lett*. **1997**, 139−140. (c) Yamamoto, T.; Komarudin, D.; Arai, M.; Lee, B.-L.; Suganuma, H.; Asakawa, N.; Inoue, Y.; Kubota, K.; Sasaki, S.; Fukuda, T.; Matsuda, H. *J. Am Chem. Soc*. **1998**, *120*, 2047−2058. (d) Yamamoto, T.; Otsuka, S.; Namekawa, K;, Fukumoto, H.; Yamaguchi, I.; Fukuda, T.; Asakawa, N.; Yamanobe, T.; Shiono, T.; Cai, Z. G. *Polymer* **2006**, *47*, 6038−6041.
(15) (a) Pope, M.; Swenberg, C. E. *Electronic Processes in Organic Crystals and Polymers*, 2nd ed.; Oxford University Press: 1999. (b) Marcus, R. A. *Rev. Mod. Phys.* **1993**, *65*, 599. (c) Hutchison, G. R.; Ratner, M. A.; Marks, T. J. *J. Am Chem. Soc.* **2005**, *127*, 16866−16881.
(16) (a) Bredas, J.-L.; Beljonne, D.; Coropceanu, V.; Cornil, J. *Chem. Rev.* **2004**, *104*, 4971−5004. (b) Coropceanu, V.; Cornil, J.; da Silva Filho, D. A.; Olivier, Y.; Silbey, R.; Bredas, J.-L. *Chem. Rev*. **2007**, *107*, 926−952.

10.1021/ja076235t CCC: $37.00

The close molecular contacts of conjugated oligomers appear to fall into two classes: π-stacked and herringbone.[18] Due to electrostatic interactions, π-stacks with adjacent molecules lying directly over one another are unstable with respect to stacks in which the molecules are "slipped" with respect to one another. The "slip" can be resolved into two components: a displacement in the direction of the long molecular axis ("pitch" displacement, d_P) and in the direction of the short molecular axis ("roll" displacement, d_R). Bithiazole oligomers tend to have relatively large pitch displacements leading to a π-stacked structure, whereas thiophenes tend to display larger roll translations.[18] Herringbone packing occurs under the roll displacement.[18] Polymers of the corresponding oligomers appear to follow the same pattern. Models of alkyl-substituted bithiazole polymers have no roll displacements,[16,19] whereas the current models of polythiophenes all have a "setting angle" for the conjugated main chain.[20−25] The setting angle, ϕ, is defined as the angle between the plane of the main chain and the crystallographic *a*-axis and, in a monoclinic or orthorhombic cell, is equivalent to the "roll angle", *R*, as defined in ref 18.

Conjugated oligomers and polymers exhibit polymorphism that strongly affects their electrical properties.[26−35] Thus, it is desirable to understand the causes of the polymorphism, especially as it pertains to the role of the aliphatic side chains in conjugated materials. It is well-established that conjugated oligomers display many of the electronic and structural features of their polymeric brethren, and that studies on oligomers can help our understanding of the properties of polymers.[36] In this paper, we report an extensive study of thermally induced disorder in the alkyl side groups of bithiazole oligomers, **NBTz*n*** and **NT$_2$N** (Scheme 1), that employs DSC, FTIR, MAS NMR, UV−vis spectroscopy, and XRD as a function of temperature. These measurements have been correlated with disorder-driven phase changes and thermochromism.

Scheme 1

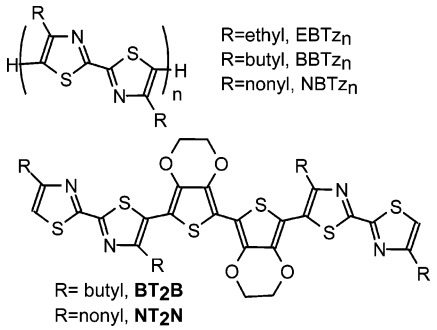

Table 1. Peak Temperatures and Heat Flow in the DSC Thermograms of Nonyl Bithiazole Oligomers and Polymer

	NBTz$_n$			
n	T_m	T_c	ΔH_{endo} (kJ/mol)	ΔH_{exo} (kJ/mol)
1	59.2	36	9.2	−9.2
2	46,[a] 95	25,[a] 73	14.2,[a] 20.1	−15.9,[a] −23.5
3	122	95	33.9	−35.2
5	140	98	25.1	−18.8
52	297	256	2.9[b]	−3.4[b]

[a] $\alpha \rightarrow \beta$ transition. [b] Per bithiazole repeat unit, uncorrected for degree of crystallinity.

Results

Thermal Properties. The DSC and TGA results of the 4,4′-dinonyl-2,2′-bithiazole series from monomer to polymer are summarized in Table 1 and Figure S-1 (see Supporting Information), respectively. There is a systematic increase in both the melting and the crystallization temperatures with increasing main-chain extension as observed by DSC. The thermal stability across the series is relatively consistent with a 10 wt % loss between 455 and 505 °C. There is an increase in the residual weight left after high temperatures with increasing main chain length. The nonyl alkyl side chains represent 60.5% of the overall molecular weight of the **NBTz** unit. It appears that with increasing length of the main chain, the pendant alkyl chains volatilize first, leaving behind the main chain residue that is stable to at least 700 °C.

The DSC of **NBTz** exhibited a single endotherm (T_m = 59.2 °C, ΔH= 9.2 kJ/ mol) and a single exotherm (T_c = 35.8 °C, ΔH = −9.2 kJ/mol) in the temperature range 0−110 °C. These thermal transitions correspond to melting and crystallization of **NBTz**, and the separation between the two temperatures corresponds to supercooling of the melt. Figure 1 depicts the DSC of the **NBTz$_2$**, the dimer of **NBTz**, taken at scan rates of 10 and 2 °C/min. Two large endotherms at 46 °C (ΔH = 14.2 kJ/mol) and 95 °C (ΔH = 20.1 kJ/mol) (heating rate = 2 °C/min) are observed upon heating across the temperature window from 0 to 110 °C, and two main peaks were also observed on the cooling cycles at 73 (−23.5 kJ/mol) and 25 °C (−15.9 kJ/mol). On the first scan, a smaller endotherm is observed at 57 °C (heating rate = 10 °C/min), but this peak is not seen in later scans. The higher temperature peak corresponds to the melting

(18) Curtis, M. D.; Cao, J.; Kampf, J. W. *J. Am. Chem. Soc.* **2004**, *126*, 4318−4328.
(19) (a) Gonzalez-Ronda, L.; Martin, D. C.; Nanos, J. I.; Politis, J. K.; Curtis, M. D. *Macromolecules* **1999**, *32*, 4558−4565. (b) Gonzalez-Ronda, L.; Martin, D. C. *Macromolecules* **1997**, *30*, 1524−1526.
(20) (a) Prosa, T. J.; Winokur, M. J.; Moulton, J.; Smith, P.; Heeger, A. J. *Macromolecules* **1992**, *25*, 4364−4372. (b) Prosa, T. J.; Winokur, M. J.; McCullough, R. D. *Macromolecules* **1996**, *29*, 3654−3656.
(21) Meille, S. V.; Romita, V.; Caronna, T.; Lovinger, A. J.; Catellani, M.; Belobrzeckaja, L. *Macromolecules* **1997**, *30*, 7898−7905.
(22) Arosio, P.; Famulari, A.; Catellani, M.; Luzzati, S.; Torsi, L.; Meille, S. V. *Macromolecules* **2007**, *40*, 3−5.
(23) (a) Yamamoto, T.; Mahmut, A.; Abe, M.; Kuroda, S.-I.; Imase, T.; Sasaki, S. *J. Poly. Sci. B Poly. Phys.* **2005**, *43*, 2219−2224. (b) Yamamoto, T.; Arai, M.; Kokubo, H. *Macromolecules* **2003**, *36*, 7986−7993.
(24) Tashiro, K.; Kobayashi, M.; Morita, S.; Kawai, T.; Yoshino, K. *Synth. Met.* **1995**, *69*, 397−398.
(25) Xie, H.; O'Dwyer, S.; Corish, J.; Morton-Blake, D. A. *Synth. Met.* **2001**, *122*, 287−296.
(26) (a) Troisi, A.; Orlandi, G. *J. Phys. Chem. B* **2005**, *109*, 1849−1856. (b) Siegrist, T.; Kloc, C.; Laudise, R. A.; Katz, H. E.; Haddon, R. C. *Adv. Mater.* **1998**, *10*, 379−382. (c) Antolini, L.; Horowitz, G.; Kouki, F.; Garnier, F. *Adv. Mater.* **1998**, *10*, 382−385. (d) Barbarella, G.; Zambianchi, M.; Antolini, L.; Ostoja, P.; Maccagnani, P.; Bongini, A.; Marseglia, E. A.; Tedesco, E.; Gigli, G.; Cingolani, R. *J. Am Chem. Soc.* **1999**, *121*, 8920−8926.
(27) Chen, S.-A.; Ni, J.-M. *Macromolecules* **1992**, *25*, 6081−6089.
(28) Tashiro, K.; Minagawa, Y.; Kobayashi, M.; Morita, S.; Kawai, T.; Yoshino, K. *Synth. Met.* **1993**, *55−57*, 321−328.
(29) (a) Hsu, W.-P.; Levon, K.; Ho, K.-S.; Myerson, A. S.; Kwei, T. K. *Macromolecules* **1993**, *26*, 1318−1323. (b) Ho, K. S.; Bartus, J.; Levon, K.; Mao, J.; Zheng, W.-Y.; Laakso, J.; Taka, T. *Synth. Met.* **1993**, *55−57*, 384−387.
(30) (a) Bolognesi, A.; Porzio, W.; Provasoli, F.; Ezquerra, T. *Makromol. Chem.* **1993**, *194*, 817−827. (b) Bolognesi, A.; Porzio, W.; Zhuo, G.; Ezquerra, T. *Eur. Poly. J.* **1996**, *32*, 1097−1103.
(31) Zhao, Y.; Keroack, D.; Yuan, G.; Massicotte, A. *Macromol. Chem. Phys.* **1997**, *198*, 1035−1049.
(32) Liu, S. L.; Chung, T. S. *Polymer* **2000**, *41*, 2781−2793.
(33) Wang, Y.; Archambault, N.; Marold, A.; Weng, L.; Lucht, B. L.; Euler, W. B. *Macromolecules* **2004**, *37*, 5415−5422.
(34) Ong, B. S.; Wu, Y.; Liu, P.; Gardner, S. *J. Am Chem. Soc.* **2004**, *126*, 3378−3379.
(35) Causin, V.; Marega, C.; Marigo, A.; Valentini, L.; Kenny, J. M. *Macromolecules* **2005**, *38*, 409−415.
(36) (a) Müllen, K.; Wegner, G. *Electronic Materials: The Oligomer Approach* Wiley-VCH: Weinheim and New York, 1998. (b) Enkelmann, V. *Oligomers as Structural Models for Polymers*; Wiley: New York, 1998.

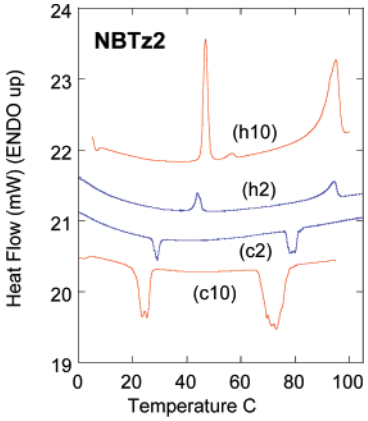

Figure 1. DSC thermograms of $NBTz_2$: (h10) heating at 10 °C/min, (c10) cooling at 10 °C/min, (h2) heating at 2 °C/min, (c2) cooling at 2 °C/min.

point of the dimer. The melting endotherm is asymmetric (skewed to low temperature), and the corresponding exotherm on the cooling cycle shows considerable "fine structure", a shoulder and three distinct peaks. The lower temperature exotherm is split into two peaks on the first cycle, but appears as a skewed peak in later scans. We shall argue later that the first large endotherm is related to a phase change (α to β) that is driven by the disordering of the pendant side chains. In poly(3-alkylthiophenes), P3ATs, this phase change has been previously ascribed to "side-chain melting."[29,31] The complex behavior on cooling may represent the formation of mesophases in the melt just before the sample crystallizes.[19b]

The DSC thermograms of the nonyl-substituted trimer (**$NBTz_3$**) and pentamer (**$NBTz_5$**) exhibited single broad endotherms upon heating (122 and 139 °C, respectively) and after successive heating and cooling cycles. Upon cooling, the pentamer showed a single broad exotherm at 90 °C, but the trimer exhibited a different behavior from that of either the dimer or the pentamer. The DSC thermogram of **$NBTz_3$** is shown in Figure 2a. The initial cooling of the sample from the melt at 10 °C/min yields a main crystallization exotherm at ~95 °C. However, a sharp and distinct exotherm at ~92 °C appears as a shoulder on the first broad peak. Two subsequent heating cycles (5 and 2 °C/min) each produce a single, broad endothermic peak, while the slower cooling cycles begin to separate the crystallization exotherm into two resolved peaks. Upon cooling from the isotropic melt, the phase transition at ~95 °C represents the crystallization of the oligomer to the β-phase; and the smaller exotherm at 92 °C represents a phase transition (β to α) accompanied by the ordering of the nonyl side chains. Apparently, the bulk trimer (obtained by precipitation) is trapped in the β-phase, and when initially heated to ~122 °C, the measured enthalpy change (19 kJ/mol) is representative of the heat of fusion ($\beta \rightarrow$ I, isotropic melt). After the sample is allowed to slowly cool from the melt, it first crystallizes in the β-phase at 95 °C and then quickly transitions to the α-phase at 92 °C, and the combined heat of these two processes is −35.2 kJ/mol. Subsequent heating cycles do not show two separate endotherms associated with the two observed exothermic transitions—only a single broad endotherm is observed. However, the enthalpies of the endotherms of the second and third scans are larger (33.9 kJ/mol) relative to the initial enthalpy change and approach the value seen for the initial exotherm. We propose that the $\alpha \rightarrow \beta$ phase transition is kinetically slow until the melting temperature is nearly reached. Thus, the endotherm due to the $\alpha \rightarrow \beta$ phase transition blends in with the melting endotherm, and the energy of the $\alpha \rightarrow \beta$ phase transition (~15 kJ/mol) is added to the enthalpy of melting (~19 kJ/mol).

The effect of the alkyl chain length was investigated using the trimer (three bithiazole units, six thiazole rings) as a base, main-chain unit. Along with the previously presented temperature dependence of the nonyl derivative, **$NBTz_3$**, the thermal behavior of the hexyl and ethyl substituted trimers (**$HBTz_3$**, and **$EBTz_3$**, respectively) were explored (Figures 2, parts b and c). There is a significant effect of the side chain length on the mp: 158, 162, and 122 °C, respectively, for the ethyl, hexyl, and nonyl-substituted trimers, and the crystallization temperatures follow a similar trend. The melting endotherms of the nonyl and ethyl derivatives are broad and somewhat asymmetric. The melting endotherm of the hexyl derivative clearly shows that it is composed of two peaks, and two peaks are likewise discernible in the crystallization exotherm. These results support the hypothesis that the hexyl and nonyl *trimers* undergo an $\alpha \rightarrow \beta$ phase transition near the melting point, whereas the corresponding transition temperatures in the nonyl bithiazole *dimer* are well separated. Thus, the separation between the $\alpha \rightarrow \beta$ and $\beta \rightarrow$ I transitions depends on the lengths of both the main chain and the pendant side chains.

The thermal behavior of the bithiazole-bis(ethylenedioxythiophene) co-oligomers, **NT_2N** and **BT_2B** (Scheme 1), is similar to that of the bithiazole oligomers. **BT_2B** has one first-order transition in both heating and cooling cycles: a broad endothermic peak (247 °C, $\Delta H = 61$ kJ/mol) in the heating cycle was assigned to the melting (K → I) transition and an exothermic peak (201 °C, $\Delta H = -57$ kJ/mol) in the cooling cycle was attributed to the reverse crystallization process. However, the DSC thermogram of **NT_2N** (Figure S-2) displays two endothermic (91 °C, $\Delta H = 60$ kJ/mol and 175 °C, $\Delta H = 63$ kJ/mol) and two exothermic peaks (157 °C, $\Delta H = -70$ kJ/mol and 81 °C, $\Delta H = -64$ kJ/mol) in the heating and cooling cycles, respectively. The peaks were reproducible even in the fourth scan and are assigned to the $\alpha \rightarrow \beta$ and $\beta \rightarrow$ I transitions, respectively. It is interesting to note that in both **NT_2N** and **$NBTz_2$** the enthalpy of the $\alpha \rightarrow \beta$ transitions are nearly equal to their respective $\beta \rightarrow$ I transitions, although the enthalpies associated with **NT_2N** are about three times as large as those for **$NBTz_2$**.

FTIR Spectra. FTIR studies were conducted to determine any changes in the vibrational modes as a function of temperature in order to help establish the cause of the observed thermal behavior. The vibrational modes for oligo and polythiophenes have been assigned by several investigators.[37] Given the C_{2h} point group of the 4,4′-dialkyl-2,2′-bithiazole molecule in its trans-anti-planar conformation, the gerade (g) modes are exclusively Raman active, whereas the ungerade (u) modes are only IR active. Figure S-3 depicts the high and low-temperature IR scans for the dimer, **$NBTz_2$** (see Supporting Information).

Many of the fundamental vibrations of unsubstituted and 4-subtituted bithiazoles and its oligomers have been studied and described, but several key vibrations experimentally observed

(37) (a) Louarn, G.; Trznadel, M.; Buisson, J. P.; Laska, J.; Pron, A.; Lapkowski, M.; Lefrant, S. *J. Phys. Chem.* **1996**, *100*, 12532−12539. (b) Trznadel, M.; Zagorska, M.; Lapkowski, M.; Louarn, G.; Lefrant, S.; Pron, A. *J. Chem. Soc.-Faraday Trans.* **1996**, *92*, 1387−1393. (c) Zerbi, G.; Chierichetti, B.; Inganas, O. *J. Chem. Phys.* **1991**, *94*, 4637−4645.

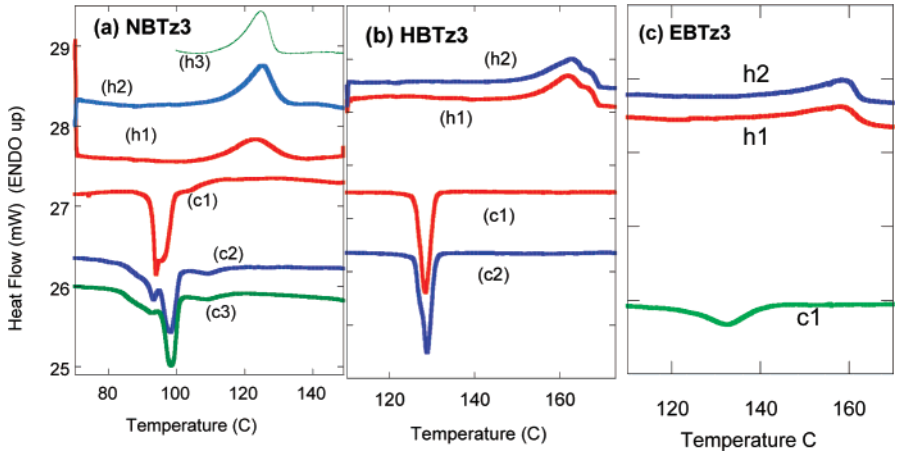

Figure 2. DSC thermograms for alkylbithiazole trimers (ABTz3) where the alkyl group (A) is as follows: nonyl (a), hexyl (b), and ethyl (c). Heating and cooling rates are 2 °C/min.

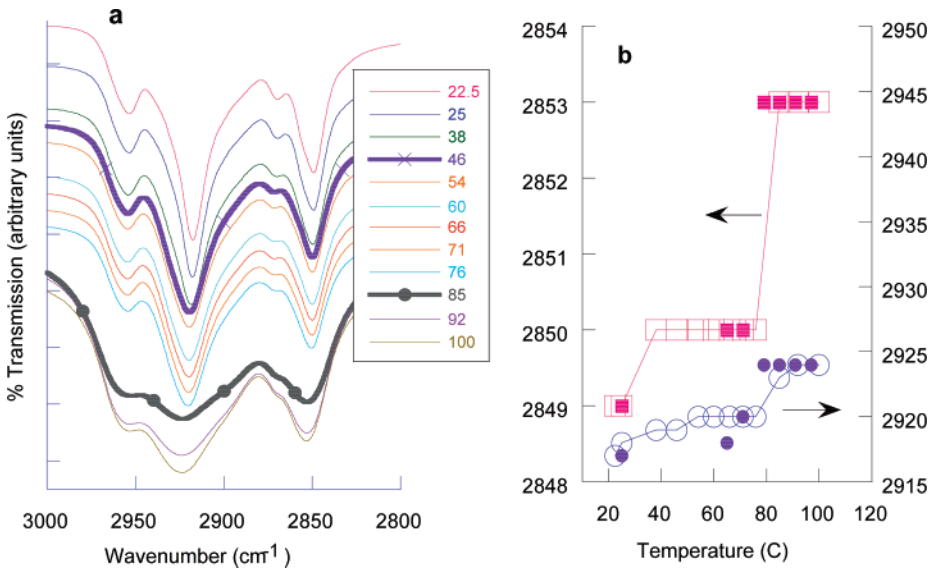

Figure 3. FTIR spectra of **NBTz$_2$** as a function of temperature. (a) C−H stretching region as a function of temperature. Bold lines correspond to the temperatures of the observed DSC peaks. (b) Frequencies of υ_{as} (squares) and υ_{sym} (circles) vs temperature. Open symbols-heating, filled symbols-cooling.

in this study had yet to be assigned. Therefore, IR frequencies were calculated based on the optimized geometry of a bithiazole dimer substituted with butyl groups in the 4 and 4′ positions (Spartan '04 quantum mechanical package).[38] The atomic coordinates of the ethyl substituted bithiazole dimer (**EBTz$_2$**)[18] were imported into the Spartan software program, and the ethyl groups were extended to butyl by adding additional methylene groups in the all-trans conformation. The geometry was then optimized using the Hartree−Fock Ab Initio methodology with the 3-31G* basis set. The individual thiazole rings remained essentially coplanar, but the outer rings deviated slightly from planarity (dihedral angle = 0.03°), while the dihedral between the inner rings remained at 180°. IR frequencies were then calculated based on this optimized geometry. The calculated and experimental IR spectra are shown in Figure S-4, and the observed frequencies and assignments are shown in Table S-1 (see Supporting Information).

Figures 3 and 4 show the IR spectra of a $CHCl_3$ solution-cast film of **NBTz$_2$** as a function of temperature in the range 22−100 °C, a range that encompasses all of the thermal transitions observed in the DSC. The C−H stretching region is depicted in Figure 3a, in which the bold lines correspond to the spectra taken at the DSC transition temperatures. The frequencies of the symmetric and asymmetric CH_2 vibrations are plotted in Figure 3b. As the temperature increased, there were fairly abrupt changes in both frequencies, from 2916 to 2920 cm^{-1} (υ_{as}) and from 2849 to 2850 cm^{-1} (υ_{sym}) at the $\alpha \rightarrow \beta$ transition temperature (~46 °C); and, near 85 °C (onset of the $\beta \rightarrow$ I transition), the frequencies again shift; from 2920 to 2924 cm^{-1} (υ_{as}) and from 2850 to 2853 cm^{-1} (υ_{sym}). These frequency shifts were reversible as the temperature was lowered (Figure 3b).

Figure 4a shows the IR spectra in the region from 1550 to 1350 cm^{-1} as the temperature is ramped from RT to 100 °C. This region includes the ring stretching/ breathing mode at 1514 cm^{-1} and the mode at 1469 cm^{-1} that arises from C═N/ C═C stretch coupled to a CH_2 wag. There is a continual decrease in the intensities of each of these bands as the temperature was increased from 22 to 46 °C. In addition to the decrease of intensity, the 1469 cm^{-1} band, having a contribution from the alkyl chain vibrations, shifts abruptly to 1466 cm^{-1} at the low temperature thermal transition and gradually drifts to 1464 cm^{-1}

(38) Wavefunction; 2002 and 2004 ed.; 18401 Von Karman Avenue, Suite 370, Irvine, CA 92612: Irvine, 2004.

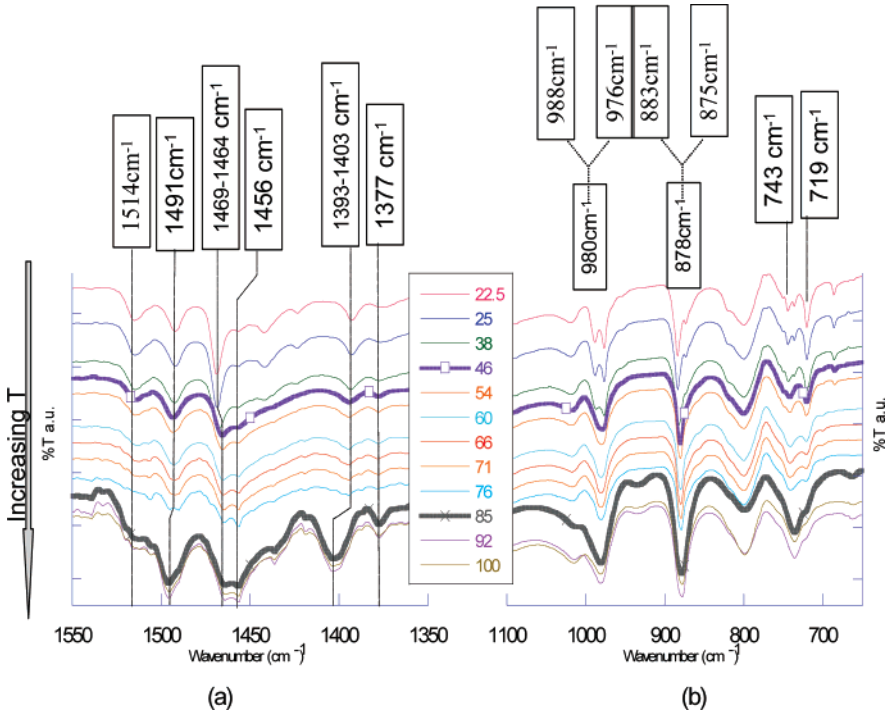

Figure 4. Temperature dependence of the FTIR of $NBTz_2$ in the (a) 1550−1350 cm^{-1} and (b) 1100−650 cm^{-1} region (alkyl bending region). The bold lines correspond to the temperatures of the observed DSC peaks.

through the melting temperature. Similarly, the 1393 cm^{-1} band, with components due to aliphatic C−C stretch and C−H wag as well as ring C−N stretch, undergoes an abrupt shift in frequency to 1403 cm^{-1} at the melting temperature.

The region between 1100 and 650 cm^{-1} is shown in Figure 4b. The aliphatic side chain modes that are coupled to the ring C−N stretches, located at 988 and 976 cm^{-1}, coalesce into one peak, centered at 980 cm^{-1} at the low-temperature transition. A similar trend is seen for the C−H wag modes at 883 and 875 cm^{-1} as these peaks merge to give a single absorption at 878 cm^{-1}. Finally, the peak at 743 cm^{-1} that is coupled to a side chain vibration grows in intensity with increasing temperature, whereas the ring C−S−C deformation at 719 cm^{-1} gradually decreases in intensity as the temperature is raised.

The 1380−1200 cm^{-1} region is especially important as the weak CH_2 wagging modes that appear in this frequency range are very sensitive to the local environment of the methylene groups. In particular, these modes have been correlated with the local conformations of the alkyl chain, e.g., all trans (ttt), gauche−trans−gauche (gtg), etc.[39] Figure 5 shows this spectral region for three temperatures, 22.5, 38, and 55 °C. The first two temperatures lie below the $\alpha \rightarrow \beta$ phase transition, and the last lies just above this transition. The 1329, 1295, 1290, and 1229 cm^{-1} peaks arise from the all-trans conformation of the nonyl chain, whereas the 1363 cm^{-1} peak is assigned to a gtg′ (kink) conformation and the 1340 cm^{-1} to a gtt (end gauche). From 22.5 to 38 °C, the intensities of the ttt peaks decrease slightly along with a concomitant increase in the intensities of the gtg′ and gtt peaks. After the $\alpha \rightarrow \beta$ transition, the intensities of the ttt peaks decrease drastically, while those connected to gauche conformations continue to grow. Figure S-5 shows the corresponding spectra of the samples held at 76 and 85 °C, i.e.,

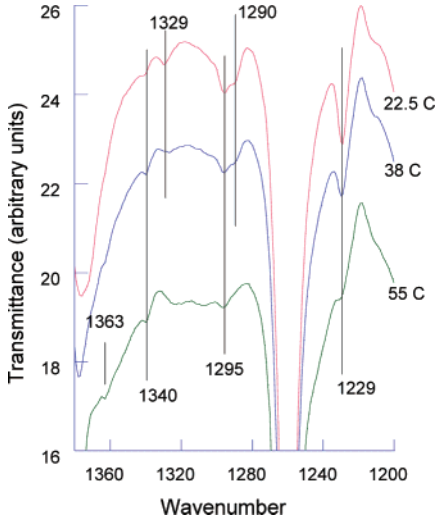

Figure 5. FTIR spectra of $NBTz_2$ in the 1380−1200 cm^{-1} region showing the changes in the CH_2 wagging and rocking modes asa function of temperature.

just below the melt temperature (see Supporting Information). Compared to the spectra in Figure 5, the peaks due to the ttt conformations have all but disappeared and gg, gtg, and gtg′ peaks have gained intensity. The major differences between the 76 and 85 °C spectra are the relative increase in the strength of the gg and gtg and the decrease in the gtg′ peak.

Solid-State NMR. Figure 6 shows the solution NMR spectra of the nonyl-substituted co-oligomer, **NT_2N**, and the nonyl bithiazole dimer, **$NBTz_2$**. The highest field triplets ($\delta \approx 0.07$ ppm) arise from the terminal methyl groups of the nonyl side chains. The two sets of triplets between 2.5 and 3.0 ppm are due to the inequivalent α-CH_2 groups located at the "inner" and "outer" (4- and 4′-) positions of the bithiazole ring. The β-CH_2 groups appear as a multiplet near 1.6 ppm. Although the inner and outer β-methylene groups are also in nonequivalent

(39) Hagemann, H.; Strauss, H. L.; Snyder, R. G. *Macromolecules* **1987**, *20*, 2810−2819.

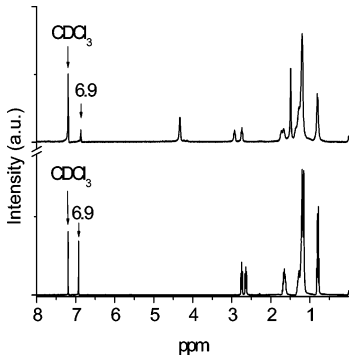

Figure 6. ^{1}H NMR spectra of **NT_2N** and **$NBTz_2$** in $CDCl_3$ solution (a.u. = arbitrary units).

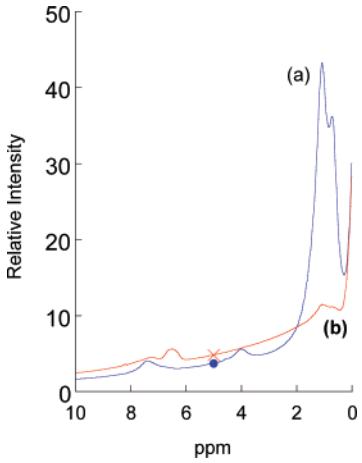

Figure 7. Solid-state MAS ^{1}H NMR spectra of (a) **NT_2N** and (b) **$NBTz_2$** at RT normalized to a silicone grease internal standard (−0.08 ppm).

environments, their signals are not resolved, nor are the peaks near $\delta = 4.3$ ppm due to the $-OCH_2CH_2O-$ substituents on the central EDOT rings of **NT_2N**. The remaining "internal" methylene groups (C3−C8) produce the set of unresolved peaks in the region 1 to 1.5 ppm. The terminal, aromatic proton of the bithiazole group appears as a singlet at 6.9 ppm in both **NT_2N** and **$NBTz_2$**.

Figure 7 displays the room-temperature MAS-^{1}H NMR spectra of **NT_2N** and **$NBTz_2$**, normalized to a silicone grease (PDMS) internal standard. The low T_g and amorphous structure of PDMS allows significant motion of the methyl groups; consequently, the grease signal is "solution-like", i.e., relatively sharp and temperature independent, and serves as a convenient internal standard. As Figure 7 shows, the normalized signals due to the aromatic protons of **NT_2N** and **$NBTz_2$** have comparable intensity, but the peaks due to the methylene and methyl groups are much more intense in the **NT_2N** spectrum. We interpret this phenomenon as there being more space for librational motion in the **NT_2N** crystal as compared to **$NBTz_2$** (see Discussion Section).

Figure 8a shows the variable-temperature MAS-NMR spectra of **$NBTZ_2$** from 30 to 84 °C, a temperature range that spans the first DSC transition at ∼45 °C. At RT, the aromatic proton resonance found at 6.9 ppm in solution has split into a doublet located at 7.25 and 6.50 ppm in the solid. As the temperature was increased to above the first DSC transition, these two peaks were replaced by one peak at 6.33 ppm (see inset in Figure 8a). The intensities of the peaks vary only slightly in this temperature range. The aromatic proton signals in the MAS NMR spectra of **NT_2N** behaved similarly (Figure S-7). The peak shifted downfield relative to the solution spectrum and split into a partially resolved doublet (7.3 and 7.4 ppm) at RT. The intensity of the aromatic proton peaks increased with temperature up to 72 °C, while the relative intensity between two peaks remained almost the same. Above 72 °C, no significant change occurred until above the temperature of the first DSC transition (91 °C), at which point the intensity of the two peaks gradually decreased as a new peak at 6.55 ppm grew in strength. Above the melting temperature, the intensities increase by an order of magnitude as the molecules can tumble in the isotropic liquid phase. The spectra of **NT_2N** show the onset of oxidation above the mp. (Figure S-7). The extra peaks that appear at 7.0 and 7.3 ppm remain in the NMR spectrum even when the cooled sample is dissolved in chloroform.

As Figure 8a shows, relative to the unchanging height of the aromatic proton peaks, the peaks due to the alkyl side chain protons become narrower, more resolved, and increased in height as the temperature was increased. These effects are the result of increased molecular motion in the side chains while the rigid main chains remain relatively fixed within the crystal lattice. As the temperature is increased above the mp (94 °C), the intensities of all peaks increase by over an order of magnitude and become much sharper (Figures 8b and S-6). The relative intensities as a function of temperature are plotted in Figure 9 and Figure S-8 (see Supporting Information).

Variable-Temperature XRD. The temperature-dependent XRD spectra for a powder sample of **$NBTz_2$** are shown in Figure 10 in the temperature range from 25 to 105 °C, a range which includes the two transitions observed in the DSC measurements. The diffractograms at 25 and 55 °C in random and preferred orientations are shown with expanded ordinates in Figures S-9 to S-12 (see Supporting Information). As the sample temperature was raised from 25 to 45 °C, no discernible peak sharpening or broadening was observed, indicative of no changes of the crystallite size, morphology, or extent of ordered domains. At 55 °C, the temperature of the first DSC transition, an abrupt shift of the lamellar *d*-spacing was observed, from 25.14 to 26.26 Å. This distance corresponds roughly to the lateral distance between the main chains, separated by the alkyl side chains (d_{100}). The higher order reflections, (2,0,0) and (3,0,0), shift accordingly from 12.61 to 13.14 Å and 8.36 to 8.76 Å, respectively. This abrupt shift points to a solid-state phase change that we have labeled $\alpha \rightarrow \beta$.

As the temperature was raised above the melting point of the sample (95 °C as determined by DSC measurements) to 105 °C, all reflections disappeared as expected for an isotropic liquid. As the temperature was lowered and the sample recrystallized, the XRD pattern showed that the β-phase had formed in a preferred orientation relative to the substrate (see Figures S-11 and S-12 of the Supporting Information). Cooling through the lower transition temperature caused a phase change back to the α-phase, which also was formed in a preferred orientation relative to the substrate (see Figures S-9 and S-10 of the Supporting Information). In the preferred orientations, the intensities of the (*0kl*) lamellar reflections drop to near zero, indicating that the orientation of the crystallites formed by crystallizing the molten film have the *0kl* planes lying essentially perpendicular to the substrate surface. Therefore, those *hkl* reflections with nonzero *kl* components are relatively stronger

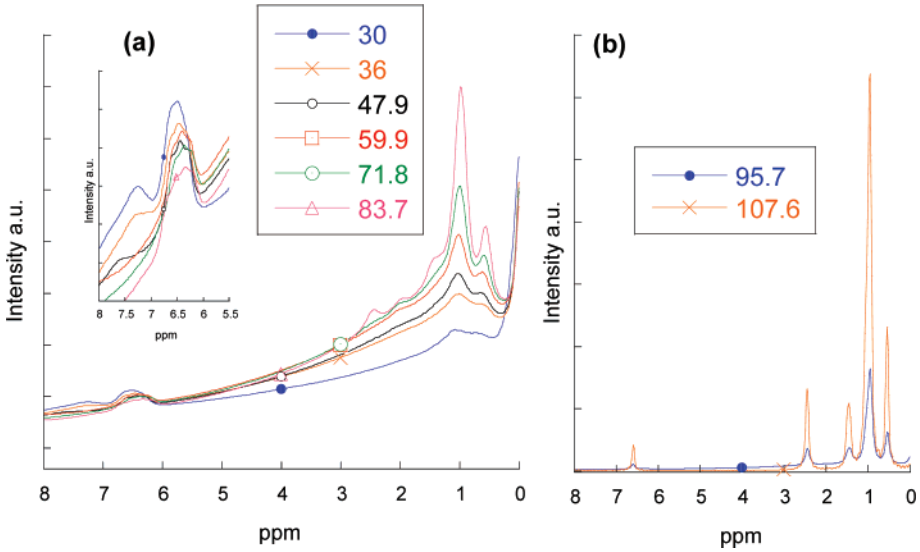

Figure 8. (a) SS-MAS-^{1}H NMR spectra of $NBTz_2$ taken at temperatures from 30 to 83.7 °C (from below to above the low-temperature DSC transition). (b) As in (a), but from below the mp to above the mp. The scale in part (a) is 20× that in part (b). All spectra are normalized to a silicone grease peak near −0.08 ppm.

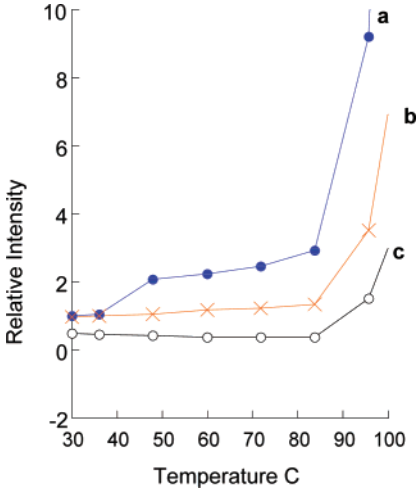

Figure 9. Relative intensities of (a) "internal" (C3−C8) methylene protons, (b) α- (C1) methylene protons, and (c) β-(C2) methylene protons as a function of temperature.

in the XRD diffractograms of the preferred orientations. The reflections for the 25 and 55 °C random orientations were indexed with the program Jade 8.[40] Because of the relatively low number of resolved peaks in the powder patterns, the indexing was not unique. However, the crystal structures of several alkyl-substituted bithiazoles are known, and typically consist of a long axis (lamellar spacing), a short axis (5−6 Å, the π-stacking axis), and an axis of intermediate length.[18] This knowledge, along with the calculated density, was used to select the most probable cell of the several that were produced by the indexing program. The resulting cell parameters are listed in Table 2. These cell parameters are a function of processing history of the sample and show variations of several percent, depending on the how the sample was prepared, e.g., crystallization from the melt vs a solvent, solvent casting on a substrate vs precipitation, etc. Tables S-2 and S-3 list the observed values of 2θ, their assigned indices, and the observed and calculated d-spacings for the randomly oriented powders at 25 and 55 °C, obtained by precipitation (see Supporting Information).

Powder X-ray diffraction patterns of **NT_2N** were obtained also at various temperatures as shown in Figure S-14 (see Supporting Information). These variable-temperature X-ray patterns also showed two transitions, between 100 and 110 °C (α → β), and between 170 and 180 °C (β → I), corresponding to the transitions observed in the DSC and variable-temperature solid-state NMR spectra. At room temperature, two low-angle diffractions at $2\theta = 3.96°$ ($d = 22.30$ Å) and 4.5° ($d = 19.63$ Å) were observed. The ratio of peaks was ca. 1:2. As the temperature was increased, the intensity of the 3.96° peak gradually diminished, but then increased abruptly and shifted to $2\theta = 4.0°$ ($d = 22.08$ Å) above 110 °C, i.e., at the α → β phase transition. Apparently, solution cast films deposit both α and β phases, and the transformation of the β phase into the thermodynamically stable α phase is slow at room temperature. The rate of β → α conversion increased as the temperature was raised, but the conversion into the α-form was not complete by the time the sample reached the temperature, $T_{\alpha\beta}$ at which the β-phase becomes the thermodynamically stable form. At $T_{\alpha\beta}$, the α-phase transforms rapidly into the β-phase, and the intensity of the $2\theta = 4.0°$ peak increased as the 4.5° peak disappeared. The peak at $2\theta = 24.28°$ ($d = 3.75$ Å) in the **NT_2N** diffractograms also shifted to smaller diffraction angles with increasing temperature up to 90 °C, and then at 110 °C the peak was replaced with a new peak at $2\theta = 24.70°$ ($d = 3.69$ Å) that also shifted to smaller angles with increasing temperature. At 180 °C, no peaks were observed, indicating that the **NT_2N** had melted. Thus, the temperature dependence of the XRD of **NT_2N** shows that it undergoes a phase change at the lower DSC endotherm.

Solution cast films of **$NBTz_2$** also produced a mixture of both phases. Precipitated powders or annealed films showed only the larger angle lamellar peak, but solution cast films always showed both the larger and lower angle lamellar peaks (see Figure S-15 of the Supporting Information). As the solvent evaporates from solution during the film-casting process, a nematic mesophase may develop over a very narrow range of

(40) Program, Jade 8, Materials Data Inc. (MDI), 1224 Concannon Blvd., Livermore, CA 94550.

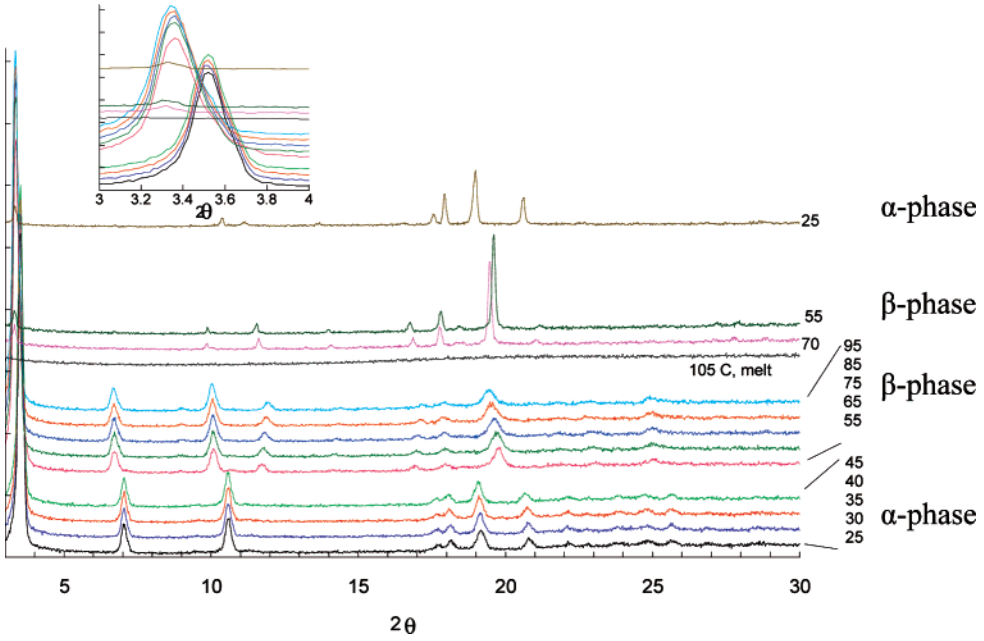

Figure 10. Temperature-dependent XRD of $NBTz_2$ polycrystalline powder, heating and cooling cycles. Inset depicts the expanded (*1,0,0*) lamellar region. Labels on the right describe the proposed phase behavior across the temperature profile.

Table 2. Cell Parameters Derived from the XRD of $NBTz_2$ in the Random Orientations of the α- and *β*-Phases at 25 and 55 °C, Respectively[a]

phase	*a* (Å)	*b* (Å)	*c* (Å)	α (deg)	*β* (deg)	*γ* (deg)	*V* (Å^3)	ρ_c (g/cm^3) (*Z*)
α	25.12	5.16	19.70	90.0	91.8	90.0	2552	1.09 (2)
β	29.40	9.42	15.29	136.3	92.8	105.8	2617	1.06 (2)
NBTz[b]	45.83	4.73	11.39	90.0	100.64	90.0	2428	1.10 (4)

[a] To permit easier comparison with each other and with polymer data, the cell parameters have been transformed from the cell as reported by the indexing program, Jade, by interchanging the a- and c-axes (α-phase) and by interchanging the a- and b-axes (*β*-phase)and transforming the angles appropriately. [b] Reference 18.

conentrations.[19b] The formation of the *β*-phase from the mesophase may be kinetically favored; and, once formed, the *β* phase is slow to revert to the thermodynamically stable α-phase. In this respect, the XRD pattern of the α-phase in the preferred orientation (Figure S-10 of the Supporting Information) showed a remnant of the *β*-phase, and the fine structure in the crystallization exotherms also suggests the presence of mesophases.

Variable-Temperature UV−Vis Spectra. The UV−vis spectra of a solution-cast film of **$NBTz_2$** as a function of temperature are shown in Figures 11 and 12. The room-temperature spectrum has a λ_{max} of 411 nm and distinct shoulders at 433 and 468 nm. As the temperature was increased, there was virtually no observable change until 45 °C, at which point there was an abrupt shift in λ_{max} to 406 nm with a slight diminution of the peak height; the 433 nm shoulder essentially disappeared while the wavelength of the 468 nm shoulder moved to 464 nm with a considerable decrease in its intensity. An expanded view of the spectra displays a distinct isosbestic point at 401 nm (Figure S-16 of the Supporting Information). We attribute the observed changes in this temperature range to the α → *β* phase transition previously established to occur near 44 °C.

Figure 12 shows the spectra recorded from 60 to 100 °C. The intensity of the 406 nm peak slowly decreased between 60 and 84 °C, and the shoulder at 459 nm continued to shift to

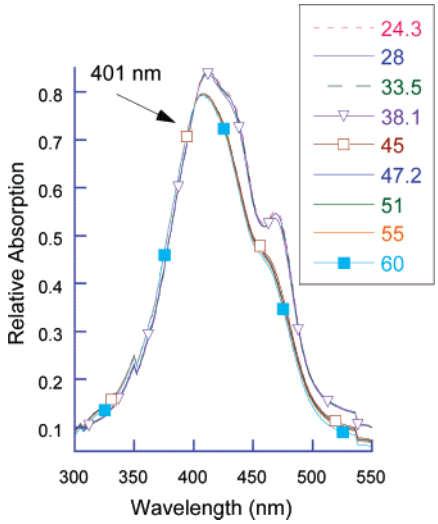

Figure 11. UV−vis spectra of $NBTz_2$ at the indicated temperatures.

longer wavelengths until it appears 470 nm at 89 °C; then it abruptly disappeared at 90 °C. There is also a long-wavelength "foot" centered at about 545 nm that is constant in position and intensity until it disappears between 88 and 90 °C. At ~84 °C, λ_{max} began to shift to lower values as a new peak started to grow in at 365 nm, and there appears to be an isosbestic point near 390 nm, possibly correlated with the *β* → I (melting) detected by DSC at 95 °C. However, as shown in the expanded view of the 390 nm region (Figure S-17 of the Supporting Information), the graphs of the spectra recorded between 60 and 80 °C are essentially parallel because the high-energy peak at 365 nm has not started to grow in. Between 80 and 100 °C, the 365 nm peak starts to grow in and an isosbestic point is seen (the small deviations from an ideal isosbestic point probably arise from imperfect baseline adjustment as the opacity of the film changes during melting).

The UV−vis spectra of the nonyl-substituted trimer and pentamer, **$NBTz_3$** and **$NBTz_5$**, and the hexyl-substituted trimer,

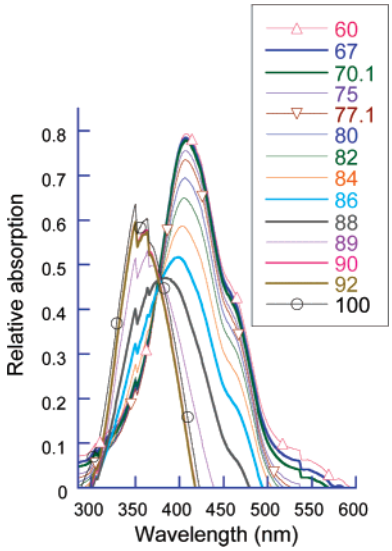

Figure 12. UV−vis spectra of $NBTz_2$ at the indicated tempuratures. The spikes near 350 and 360 nm are instrumental artifacts.

$HBTz_3$, showed behavior similar to that seen for **$NBTz_2$**: initial heating caused a diminution of the intensity of λ_{max} but the low-energy, solution-like peak did not appear until the temperature was close to the mp as determined by DSC. At that point, a more or less good isosbestic point was observed (see, for example, Figure S-18 of the Supporting Information).

The bithiazole-EDOT co-oligomer showed temperature-dependent UV−vis spectra very similar to those of **$NBTz_2$** (Figures S-19 and S-20 of the Supporting Information). The low-temperature spectra of **NT_2N** display three prominent peaks at 467, 496 (λ_{max}), and 535 nm. As the temperature was increased above the first thermal transition ($\alpha \rightarrow \beta$) at 91 °C, the fine structure was replaced by a single "foot" located at ~565 nm, although the now featureless envelope hardly changed position. As the second thermal transition ($\beta \rightarrow$ I) at 157 °C was traversed, the peak height decreased and the λ_{max} shifted from 485 to 466 nm and the foot at 565 nm disappeared. The spectra of molten **NT_2N** and **$NBTz_2$** each have a weak peak at 584 nm that may be due to a forbidden transition, e.g., $S_0 \rightarrow T_1$.

Discussion Section

Thermal Behavior. Multi-endothermic peaks have been observed in liquid crystals (LC),[41] but an examination of the melting/crystallization process of our materials under a polarizing optical microscope gave no evidence for liquid-crystalline textures in our samples. For example, **NT_2N** crystallized from the melt at 148 °C, and then no significant change was observed as the sample was cooled to room temperature. It is possible that LC domains are formed in very narrow temperature ranges near the mp and are responsible for the fine structure observed in the DSC traces. In addition, the LC domains may be too small to be imaged except with a more powerful technique, e.g., AFM.[42] However, as the following discussion will amplify, our thermal data for the oligomers are well accounted for by postulating that the crystalline solids may undergo a phase change driven by thermally induced disorder in the side chains. This phase change is observed only if the lengths of the conjugated core ("main chain") and pendant alkyl side chains are within certain bounds. We do not have sufficient data to quantitatively delineate these boundaries, but the following qualitative argument can explain our observations.

It is well-known that rigid-rod molecules, e.g., oligothiophenes, -acenes, -thiazoles, and so forth, tend to be high melting solids with the mp increasing and solubility decreasing with increasing length of the conjugated chain. These observations point to strong interchain attractions that are proportional to the number of rings in the chain. Addition of alkyl side chains decreases the mp and increases the solubility. For a given main chain length, the mp tends to decrease as the length of the side chain increases. In other words, the weaker alkyl−alkyl attractions "dilute" the stronger ring−ring attractive interactions. Nevertheless, attractive alkyl−alkyl interactions among ordered ("crystallized") side chains do add stability to the crystal structure, as exemplified by the melting points of the ethyl, hexyl, nonyl series, **$EBTz_3$**, **$HBTz_3$**, and **$NBTz_3$**: 158, 162, and 122 °C, respectively. The side-chain interactions may even be the factor that determines the given crystal structure (crystal system or space group) of a particular compound.

There have been many studies that have shown that the degree of side-chain disorder is increased at elevated temperatures. For example, the concentration of gauche defects in the all-trans, extended conformation of the side chains in crystalline normal alkanes and P3ATs grows as the temperature is increased.[25,27,29a,39,30b] As the concentration of gauche defects increases, the effective volume of the alkyl side chains increases, putting an internal strain on the crystal structure. The main chain attractions resist expansion of the unit cell. If the side-chain length is small, then the side-chain pressure is not sufficient to disrupt the cell structure until the mp is reached, at which point the thermal disorder completely overcomes the solid-state lattice energy. Increasing the length of the side chain, or decreasing the length of the main chain, allows the side-chain pressure to force a change in solid-state structure before the mp is reached. The change in structure is one that provides more room for the gauche conformations of the side chains, i.e., a phase change occurs. At some point, increasing the ratio of the of the side-chain to main-chain length lowers the mp to such a degree that the mp is reached without a preceding phase change, i.e., the entire structure simply melts. Only when the side-chain to main-chain ratio is optimal is a phase change observed as a low-temperature endotherm in the DSC prior to the mp.

The scenario described above is exactly analogous to what occurs in crystalline paraffins.[43] Even-numbered *n*-alkanes form monoclinic crystal structures, whereas odd-numbered *n*-alkanes crystallize in the orthorhombic system; in both structure types, the alkane chain is in the all-trans conformation. Paraffins may form a second phase at higher temperatures in which the molecules rotate as rigid rods about their long axes at temperatures below their first-order melt transition. The term "rotator" phase has been used to describe this pseudo-hexagonal crystal-

(41) (a) Tokita, M.; Funaoka, S.; Watanabe, J. *Macromolecules* **2004**, *37*, 9916. (b) Lehmann, M.; Gearba, R. I.; Koch, M. H. J.; Ivanov, D. A. *Chem. Mater.* **2004**, *16*, 374. (c) Chen, H. M. P.; Katsis, D.; Chen, S. H. *Chem. Mater.* **2003**, *15*, 2534.

(42) Zhao, N.; Botton, G. A.; Zhu, S.; Duft, A.; Ong, B. S.; Wu, Y.; Liu, P. *Macromolecules* **2004**, *37*, 8307.

(43) (a) Stewart, M. J.; Jarrett, W. L.; Mathias, L. J.; Alamo, R. G.; Mandelkern, L. *Macromolecules* **1996**, *29*, 4963−4968. (b) Maroncelli, M.; Strauss, H. L.; Snyder, R. G. *J. Chem. Phys.* **1985**, *82*, 2811−2824. (c) Jarrett, W. L.; Mathias, L. J.; Alamo, R. G.; Mandelkern, L.; Dorset, D. L. *Macromolecules* **1992**, *25*, 3468−3472.

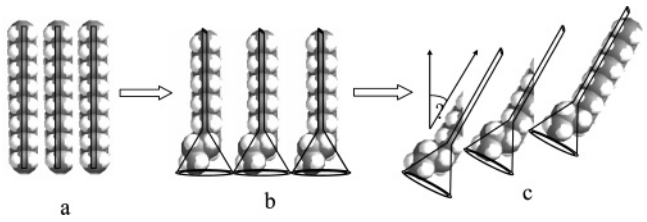

Figure 13. Effect of chain end defects (gauche conformations) forcing chain tilting to facilitate packing as temperature increases (left to right). (a) Rectangular cell, (b) increasing concentration of gauche defects, and (c) chain tilt to relieve pressure forms an oblique cell.

line modification.[44] Appearance of a "rotator phase" occurs only within a certain range of chain lengths: *n*-alkanes with carbon chain lengths $9 \leq n_{odd} \leq 43$ and $20 \leq n_{even} \leq 42$ show this phase change in DSC measurements.[45]

Similar thermal behavior has been reported by Ogawa and Nakamura for a series of α,ω-alkanediols HO−$(CH_2)_n$−OH ($n = 13-24$).[46] Except for HO−$(CH_2)_{14}$-OH, all of the α,ω-alkanediols showed two endothermic and two exothermic peaks in DSC thermograms. The first endothermic peak was assigned to a solid−solid transition and the second peak to a solid−liquid transition. In addition, Schenning and co-workers reported multiple endothermic peaks in the DSC thermograms of α,α′-linked sexithiophenes with chiral and achiral penta(ethylene glycol) chains attached at the α−ω positions of the terminal rings.[47] One of the peaks was assigned to a crystal−crystal transition based on observations with a polarizing optical microscope.

Figure 13 diagrams the effect of increasing the concentration of gauche defects on the crystal structure. As the temperature increase introduces more defects, the ends of the alkyl chains require more space. Within the confines of the rectangular cell, the chains must move apart; but at some point, the chain axes tilt to form an oblique cell that allows for better packing. If one end of the alkyl chain is tethered to a rigid main chain, the tilt of the chains would cause a lateral slip of the main chain.

Variable-Temperature FTIR. Many of the vibrational modes of **NBTz$_2$** that give rise to strong peaks showed stepwise changes at temperatures near where the DSC displayed endothermic transitions. The stepwise changes are consistent with phase changes that we have labeled α → β (44 °C) and β → I (95 °C). An increase in the intensity of the CH_2 and CH_3 bending modes located at 1456 and 1377 cm^{-1}, respectively, occurs as the mp is traversed. The melding of the 743 and 719 cm^{-1} bands may be due to a splitting of the 719 cm^{-1} peak into two peaks, ∼730 and 720 cm^{-1}, characteristic of ordered and disordered CH_2 rocking (Figure 4).[48]

More meaningful information may be obtained by considering the weak, coupled phonon modes associated with the wagging vibrations of CH_2 groups located along the side chain. There is extensive literature associated with normal alkanes and poly(ethylene) in which these vibrational modes have been assigned.[29,39] Figure 5 shows the changes in the intensities of these wagging modes in the 1380−1200 cm^{-1} region. As the temperature was raised from 22.5 °C, the intensities of the peaks associated with all-trans (*ttt*) conformations gradually decreased, whereas the intensities of the peaks associated with gauche conformations (*gtg*, *gtg′*) increased. At the α → β transition, there was a sudden drop in the height of the *ttt* peaks and a corresponding increase in the gauche conformations. Thus, it appears that the α → β transition corresponds to a change in the crystal structure that is driven or at least accompanied by an increase in the thermally induced structural disorder in the side chains. A ^{13}C−CP-MAS-NMR study of poly(3-octylthiophene), P3OT, shows that the gauche conformations are most concentrated near the C8 terminus of the side chain.[49] As the temperature was raised further, the *ttt* peaks continued to fade such that by the time the mp was reached, the concentration of the *ttt* conformation was essentially nil. As the mp was traversed, there was an increase in *gg* (adjacent gauche) and gtg′ (kink) conformations.

Solid-State NMR Spectra. NT$_2$N has only four nonyl side chains per six rings as opposed to a nonyl group on each of the four rings in **NBTz$_2$** (see chemical structures in Scheme 1). A crystal structure of **BT$_2$B**, an analog of **NT$_2$N** with butyl instead of nonyl side chains, was obtained on crystals grown from methylene chloride. The structure showed that methylene chloride of solvation was incorporated between **BT$_2$B** molecules even though the interlayer π-stacking distance was 3.53 Å, a value very similar to that of other π-stacked bithiazole oligomers.[18] This demonstrates that in the unsolvated crystal there is "excess" volume around the two EDOT rings in which nonyl side chains, attached to adjacent bithiazole rings, can gyrate. Alternatively, the single-crystal structure of 4,4′-alkyl-substituted bithiazole oligomers revealed that the alkyl chains are densely packed. As shown in Figure 7, the SS-NMR signals for the alkyl protons of **NT$_2$N** were more intense and better resolved at room temperature than those for **NBTz$_2$**, which indicates that the alkyl chains of **NT$_2$N** are more mobile. In fact, the spin−lattice relaxation time of the methylene protons in **NT$_2$N** (1 s) is half that of those in **NBTz$_2$** (2 s).

It is interesting to note that the peaks for aromatic protons of **NT$_2$N** and **NBTz$_2$**, which appeared at 6.9 ppm in the solution NMR, were shifted and split into two peaks: 7.4 and 7.3 ppm (**NT$_2$N**) and 7.25 and 6.50 ppm (**NBTz$_2$**). The peak splitting suggests the possibility of factor group splitting (Davydov splitting) arising from two translationally inequivalent molecules per unit cell. The structures of a variety of oligo-bithiazoles show the presence of more than one molecule per unit cell, so that the observation of Davydov splitting is not unexpected.[18,50] Above the α → β phase transition temperature, the there is only one peak for the aromatic protons, but an analysis of the powder XRD pattern gave a cell with $Z = 2$ (see below). If the cell does contain more than one molecule, the Davydov splitting of the NMR signal simply may be unresolved.

The thermal motion of molecules, which increases with temperature, leads to an averaging of the anisotropic interactions, with the result that the peaks of both aromatic and aliphatic protons narrow and increase in peak height. As shown in Figures 8, 9, S-7, and S-8 (see Supporting Information), the intensities

(44) (a) Dirand, M.; Bouroukba, M.; Chevallier, V.; Petitjean, D.; Behar, E.; Ruffier-Meray, V. *J. Chem. Eng. Data* **2002**, *47*, 115−143. (b) Sirota, E. B.; Singer, D. M. *J. Chem. Phys.* **1994**, *101*, 10873−10882.
(45) Broadhur.M.; Mopsik, F. I. *Bull. Am. Phys. Soc.* **1970**, *15*, 330.
(46) Ogawa, Y.; Nakamura, N. *Bull. Chem. Soc. Jpn.* **1999**, *72*, 943.
(47) Schenning, A. P. H. J.; Kilbinger, A. F. M.; Biscarini, F.; Cavallini, M.; Cooper, H. J.; Derrick, P. J.; Feast, W. J.; Lazzaroni, R.; Leclere, Ph.; McDonell, L. A.; Meijer, E. W.; Meskers, S. C. J. *J. Am. Chem. Soc.* **2002**, *124*, 1269.
(48) Qiao, X.; Wang, X.; Mo, Z. *Synth. Met.* **2001**, *118*, 89−95.
(49) Bolognesi, A.; Porzio, W.; Provasoli, A.; Botta, C.; Comotti, A.; Sozzani, P.; Simonutti, R. *Macromol. Chem. Phys.* **2001**, *202*, 2586−2591.
(50) Koren, A. B.; Curtis, M. D.; Francis, A. H.; Kampf, J. W. *J. Am Chem. Soc.* **2003**, *125*, 5040−5050.

of the C3−C8 methylene protons of **NBTz$_2$** and **NT$_2$N** increase only slightly with increasing temperature, and there is a slight change of slope in the curves near the α → β phase transition temperature (**NT$_2$N**). However, an order of magnitude increase in the intensity is seen when the solids melt. Thus, the SS-NMR spectra show that there is not a drastic change in side-chain motion during the α → β phase transition. Furthermore, the Cα and Cβ methylene protons, i.e., those tethered closest to the rigid main-chain, show the smallest intensity increase. X-ray and neutron scattering also show that the thermal motion is largest for the ends of the chain.[51] Taken together with the small intensity variation of the aromatic proton signals, this implies that the conjugated rings do not experience any significant increase in librational motion during the α → β phase change.

The most drastic change in the intensities of all peaks occurred at the respective melting points of **NBTz$_2$** and **NT$_2$N**. The similar relaxation behavior of the aliphatic and aromatic protons reveals that the actual melting of the side chains occurs at the same temperature as the melting of the conjugated core. Thus, variable-temperature solid-state NMR clearly shows that the first thermal transition is not related to the melting of the side chains but is associated with a solid−solid-phase transition. How is this observation to be reconciled with the FTIR data that clearly show an increase in the concentration of gauche defects at the α → β phase transition? The answer, of course, is that the SS-NMR is responding to a dynamical variable (the spin−lattice relaxation time), whereas the FTIR is measuring a static quantity (concentration of defects). The picture that emerges from a consideration of both data sets is that the β-phase has a large number of gauche defects, but these defects do not confer liquid-like mobility to the alkyl side chains.

Variable Temperature XRD. The XRD of the samples of **NBTz$_2$** and **NT$_2$N** as a function of temperature confirms that there is a phase transition near the temperature of the first endotherm observed in the DSC. The FTIR shows that there is a large increase in the concentration of gauche defects in the alkyl side chains at the phase change, and given the behavior of paraffins, it is reasonable suppose that the phase change is driven by the increasing side-chain disorder (vide supra and Figure 13). The powder patterns of each of the phases could be indexed to give a cell compatible with the known structures of related oligomers. In particular, these structures feature a cell with one long axis (corresponding to the lamellar separation), one short axis (related to the π-stacking direction), and an intermediate length axis. The density of the **NBTz** monomer, calculated from the single-crystal structure, is 1.10, and the higher oligomers are expected to have similar densities. This information was used to select the cell parameters listed in Table 2 from the several choices presented by the indexing program.

Furthermore, the pattern of peak intensities (especially in the $2\theta = 15-25°$ range) for both phases of the dimer, **NBTz$_2$**, is very similar to the simulated powder pattern for **NBTz** (Figure S-12 of the Supporting Information), indicating the actual molecular packing is very similar for all three structures and also resembles those found for other alkyl-substituted bithiazole oligomers. These structures all feature the bithiazole oligomers arranged in "slipped" π-stacks with an interplanar distance, $d_\pi \approx 3.5$ Å. The "slipping" has been described in terms of a "pitch" distance, d_P, in the direction of the long molecular axis and a roll distance, d_R, along the short molecular axis.[18] The total slip distance, d_{tot}, is equal to $(d_P^2 + d_R^2)^{1/2}$ and the crystallographic stacking distance (here, the *b*-axis) is $b = (d_\pi^2 + d_{tot}^2)^{1/2}$. Since d_π is essentially constant, the longer *b*-axis of the β-phase as compared to the α-phase implies a larger slip distance. Assuming a $d_\pi = 3.5$ Å, the calculated slip distances d_{tot} for the α- and β-phases are 3.79 and 8.74 Å, comparable to the measured slip distances of 3.17 and 9.26 Å for **NBTz** and **BT$_2$B**, respectively.[18] This result is precisely what one would expect based on the discussion of the phase changes of normal alkanes (see above and Figure 13). Thus, the picture that emerges from the FTIR, SS-NMR, and XRD is that the α → β transition is a side-chain disorder-driven crystal−crystal phase change that involves a slippage of the main chains relative to each other while leaving the conjugated backbone in an essentially planar conformation.

Variable-Temperature UV−Vis Spectra. The conclusion reached above is supported by the UV−vis spectra as a function of temperature. All of the 4,4′-dialkyl-bithiazole oligomers and polymers with longer alkyl groups display thermo- and solvochromism. Below their melting points, these materials are deep red, but above the mp are typically yellow. In good solvents, the color is yellow, but deepens to red or magenta as a poor solvent is added or as the temperature is lowered.[16c,23,52] The UV−vis spectra of the yellow solids above their mp are virtually indistinguishable from the spectra of solutions in good solvents where the conjugated rings are twisted with respect to each other. The main absorption peak of the red phase typically shows fine structure that has been associated with π-stacking (Davydov splitting and exciton coupling) and vibronic coupling.[17a,50,53−55] Analysis of UV−vis and emission spectra suggest that the values for the Davydov splitting (W_D) and exciton coupling (*J*) for oligobithiazoles are in the range, 200 and 80 meV, respectively.[50,56] These values are to be compared with those calculated by the Zindo/S method, which gives values of $W_D \geq 110$ meV and $J \approx 80$ meV for **NBTz**.[52] A value of 200 meV for the nearest neighbor exciton coupling constant, *J*, was measured directly from the spectra of π-dimers of BT_2B^+, and values of *J* between 250 and 500 meV were calculated from reported spectra of oligothiophene cation π-dimers.[57] For comparison, a value of $W_D = 0.3-1.0$ eV has been observed for oligothiophenes,[53,58] and comparable values have been calculated for oligothiophenes.[54] The values of W_D are strongly dependent on the relative orientations of translationally inequivalent molecules in the unit cell, whereas the exciton coupling parameter within each Davydov branch is sensitive to the relative positions of neighboring translationally equivalent molecules.[17a,52]

As shown in Figures 11 and S-19 (see Supporting Information), the α → β phase change causes only a very slight shift in

(51) Samuelsen, E. J.; Mardelen, J.; Carlsen, P. H.; Le Guennec, P.; Travers, J.-P.; Ressouche, E. *Synth. Met.* **1993**, *55−57*, 365−369.

(52) Nanos, J. I. "Synthesis, Characterization, and Structure-Property Relationships of Regio-Regular 4,4′-dialkyl-2,2′-bithiazole Oligomers and Polymers", Ph.D. Thesis, The University of Michigan, 2005.
(53) Bosisio, R.; Botta, C.; Colombo, A.; Destri, S.; Porzio, W.; Grilli, E.; Tubino, R.; Bongiovanni, G.; Mura, A.; Di Silvestro, G. *Synth. Met.* **1997**, *87*, 23−29.
(54) Beljonne, D.; Cornil, J.; Silbey, R.; Millie, P.; Bredas, J. L. *J. Chem. Phys.* **2000**, *112*, 4749−4658.
(55) (a) Spano, F. C. *Chem. Phys.* **2006**, *325*, 22−35. (b) Spano, F. C. *J. Chem. Phys.* **2005**, *122*, 234701−1 to 234701−15.
(56) Cao, J.; Kampf, J. W.; Curtis. M. D. *Chem. Mater.* **2003**, *15*, 404−411.
(57) Cao, J.; Curtis. M. D. *Chem. Mater.* **2003**, *15*, 4424−4430.
(58) Muccini, M.; Lunedei, E.; Taliani, C.; Beljonne, D.; Cornil, J.; Bredas, J.-L. *J. Chem. Phys.* **1998**, *109*, 10513.

λ_{max} of **NBTz$_2$** or **NT$_2$N**. Thus, the conjugated rings maintain their coplanarity during the phase change. However, a large slip displacement of adjacent main chains during the phase change (see above) would reduce the intermolecular orbital overlap between nearest neighbors, reduce the strength of the exciton coupling, and cause a change in the fine structure as seen in Figures 11 and S-19 (see Supporting Information).[17a,52] The single shoulder that remains on the low-energy side of the peaks may be due to Davydov splitting in the β-phase. Polarized spectra of oriented crystals would be necessary to resolve this point.

Above the $\alpha \rightarrow \beta$ transition, the peak height at λ_{max} started to decrease as the temperature was increased further, although the position of λ_{max} hardly changed. It was not until the temperature was within 5−10 °C of the mp that the intensity of the higher energy peak started to grow and an approximate isosbestic point was observed (Figures 12, S-15, and S-18 of the Supporting Information). This behavior is similar to that observed for the trimer (Figure S-16 of the Supporting Information) and pentamer as well as a large number of other conjugated oligomers and polymers.[27,59−62] The presence of isosbestic points suggests that only two phases are present: a disordered phase responsible for the high-energy peak, and an ordered phase in which the conjugated rings in the main chain librate about an averaged planar structure. The final high-temperature spectra are nearly identical to those of the corresponding solution spectra; however, for the **NBTz$_2$** and **NT$_2$N** oligomers, it is unlikely that the *onset* of the spectral changes corresponds to melting of the β-phase. For example, the diminution of the intensity of the low-energy peak starts near 70 °C for **NBTz$_2$** and about 130 °C for **NT$_2$N**. These temperatures are 24 and 105 °C below their respective melting points as determined by DSC. Also, optical microscopy of **NT$_2$N** under crossed polarizers failed to detect any noncrystalline phases in this temperature region. We propose that the root-mean-square twist angle, $|\xi|$, about the σ-bonds connecting the rings in the main chain in the β-phase increases with increasing temperature, but the increase in $|\xi|$ is not sufficient to decrease the inter-ring conjugation to the point that λ_{max} is affected (λ_{max} varies slowly as cosξ, the observed absorption envelope is a weighted average of spectra over all ξ, so slight changes in $|\xi|$ have little effect on the overall envelope).[63] However, the increased torsion is sufficient to affect the oscillator strength, so the intensity drops as $|\xi|$ increases.[52] The twist amplitude continues to increase as the temperature is raised,[64] until just below the mp, the *molecular* structure in the β-phase might resemble the "quasi-ordered phase" described by Holdcroft et al.,[65] but, unlike Holdcroft's quasi-ordered phase, the long range order characteristic of the crystalline β-phase is still present. At temperatures near the mp, the β-phase may resemble a plastic crystal.[60b] Finally, as the mp is approached, the long-range order starts to break up, and the thiazole rings twist farther out of coplanarity as the sample melts. One notes that a low-energy "foot" centered at 545 nm remains in the spectra until the mp is actually traversed. The presence of this spectral feature, characteristic of the solid state, shows that the spectral changes are occurring in the solid state, not the melt.

The spectra of the crystalline oligomers are not complicated by the presence of an amorphous phase that is always present in conjugated polymer samples. If we restrict our attention to a few degrees below the mp, then there appears to be an isosbestic point as the crystalline phase melts to the isotropic liquid because the temperature range of the melting process is too narrow to observe an appreciable shift in λ_{max} of the crystalline solid. In polymer samples, the melting process may occur over a sufficiently broad range (due to varying degrees of crystallite size and/ or perfection) that the shift in λ_{max} of the ordered solid is sufficiently large that the isosbestic point is destroyed. In this interpretation, the shift of λ_{max} of the ordered solid takes the place of the "quasi-ordered" phase proposed by Holdcroft et al.[65] The only difference in these two interpretations is that the quasi-ordered and ordered phases are replaced by one phase with a continuously varying λ_{max}. In polymers, these differing interpretations may be difficult to distinguish.

Side Chain Melting in P3ATs. Lattice energy and Monte Carlo calculations have recently been reported on P3ATs to investigate the thermochromic effects caused by changing local side chain conformations.[66] Increasing concentration of gauche distortions with increased temperatures culminated in the main chain distorting from coplanarity. Planarity of the rings was achieved only if the alkyl chains assumed the all trans conformation. In terms of thermochromism, it was proposed that the thermal energy stored within the attached alkyl chains (going from the all trans to gauche forms) reaches a point such that libration energy is transmitted to the tethered main chains, inducing the ring distortions that "dilate the frontier band gap".[60a]

The close similarity of the behavior of the bithiazole oligomers reported here to the phenomenon of side-chain melting (SCM) in certain P3ATs deserves some comment. First, what are the similarities in behavior between P3ATs and the oligomers? (1) The phenomenological observation of a low-temperature endotherm (T_{SCM}) in the DSC prior to the melting temperature (T_m) is seen only for a range of SC/MC (side-chain/main-chain) length ratios.[29,31] (2) $\Delta H_{SCM} \approx \Delta H_m$, the former quantity is the heat flow measured by DSC at T_{SCM}, and the latter is the heat flow at T_m.[21,27,65] (3) The lengths of the crystal a- and b-axes change at the T_{SCM}.[29,30,65] (4) The main chains remain planar or nearly so at the SCM transition. The major change in the UV−vis spectrum at the SCM transition is the loss of the second shoulder and retention of the lowest energy shoulder up to near the mp.[27,49,64,65,67] (5) the SCM transition for poly(3-decythiophene), P3DT, has been correlated with increased concentration of gauche defects in the SC.[30,49,64]

(59) (a) Inganas, O.; Salanek, W. R.; Osterholm, J.-E.; Laakso, J. *Synth. Met.* **1988**, *22*, 395−406. (b) Inganas, O.; Gustafsson, G.; Salaneck, W. R. *Synth. Met.* **1989**, *28*, C377−C384.

(60) (a) Yasuda, T.; Imase, T.; Nakamura, Y.; Yamamoto, T. *Macromolecules* **2005**, *38*, 4687−4697. (b) Yazawa, K.; Inoue, Y.; Yamamoto, T.; Asakawa, N. *Phys. Rev. B* **2006**, 094204−1 to 094204−12.

(61) Winokur, M. J.; Spiegel, D.; Kim, Y.; Hotta, S.; Heeger, A. J. *Synth. Met.* **1989**, *28*, C419−C426.

(62) (a) Faid, K.; Frechette, M.; Ranger, M.; Mazerolle, L.; Levesque, I.; Leclerc, M.; Chen, T.-A.; Rieke, R. D. *Chem. Mater.* **1995**, *7*, 1390−1396. (b) Leclerc, M.; Frechette, M.; Bergeron, J.-Y.; Ranger, M.; Levesque, I.; Faid, K. *Macromol. Chem. Phys.* **1996**, *197*, 2077−2087.

(63) Curtis, M. D. *Macromolecules* **2001**, *34*, 7905−7910.

(64) (a) Tashiro, K.; Ono, K.; Minagawa, Y.; Kobayashi, K.; Kawai, T.; Yoshino, K. *Synth. Met.* **1991**, *41*−*43*, 571−574. (b) Tashiro, K.; Ono, K.; Minagawa, Y.; Kobayashi, K.; Kawai, T.; Yoshino, K. *J. Poly. Sci., Poly. Phys.* **1991**, *29*, 1223.

(65) Yang, C.; Orfino, C. P.; Holdcroft, S. *Macromolecules* **1996**, *29*, 6510−6517.

(66) (a) Corish, J.; Feeley, D. E.; Morton-Blake, D. A.; Beniere, F.; Marchetti, M. *J. Phys. Chem. B* **1997**, *101*, 10075−10085. (b) Xie, H.; O'Dwyer, S.; Corish, J.; Morton-Blake, D. A. *Synth. Met.* **2001**, *122*, 287−296.

(67) Iwasaki, K.; Fujimoto, H.; Matsuzaki, S. *Synth. Met.* **1994**, *63*, 101−108.

Thermal annealing removes the metastable phase.[21] These similarities suggest that the phenomenon known as SCM may be a crystal−crystal phase transition like that in the bithiazole oligomers, and, in fact, SCM has been described previously as a crystal−crystal phase transition.[28,30a,64,68] Winokur et al. report that d_{100} increases and d_{h20} decrease most rapidly at about 50 °C, i.e., the approximate temperature where poly(3-dodecylthiophene), P3DDT, undergoes SCM, but these researchers ascribe the phase change to a crystal to mesophase (K → N) transition.[20] Levon et al. have also pointed out that, compared to the heat of melting per methylene group found for *n*-alkanes, the heat of side chain melting, ΔH_{SCM}, is too small for the observed degree of crystallinity.[29a] These workers also concluded that the octyl side chains in P3OT were ordered and densely packed, even though P3OT does not show an SCM endotherm in the DSC scans.

There are also differences between the behavior of the oligomers and polymers. Nematic mesophases have been proposed in the polymer systems.[29a,30b,49] Kinetically preferred crystallization of nematic mesophases to the β-phase and slow kinetics of the $\beta \rightarrow \alpha$ interconversion due to the higher viscosity of molten polymers can complicate interpretation of the polymer data. Some workers find no changes in the XRD patterns at the SCM transition, whereas others do.[49,69] One notes that the XRD of polymer films are often very poorly resolved, and the Bragg peaks sit atop a broad amorphous "halo" in the 15−25° range, the region where the *hkl* ($k,l \neq 0$) reflections appear in P3ATs. The lack of consistent observations may be caused by lack of resolution, especially if un-oriented films are used, and by different polymer MW, polydispersity, different degrees of regioregularity, and by the particular sample's processing history.

Conclusions

Alkyl-substituted bithiazole oligomers, **NBTz$_2$** and **NT$_2$N**, undergo a crystal−crystal phase transition that is driven by thermally induced formation of gauche defects in the side chains. The presence of an observable phase transition depends on the ratio of the length of the side chain to the main chain. MAS NMR shows that melt-like mobility in the side chains does not occur at the $\alpha \rightarrow \beta$ transition; rather, the side chains and main chains melt at the same temperature. UV−vis spectra demonstrate that the main chains remain essentially planar as the $\alpha \rightarrow \beta$ phase transition is traversed, but the conjugated backbone becomes increasingly twisted as the temperature is raised further until true melting is achieved, at which point the spectra resemble those obtained in solution. These characteristic observations are almost identical to those ascribed to the phenomenon known as "side chain melting" in P3ATs, suggesting that SCM in these polymers is also connected to a crystal−crystal phase transition.

Acknowledgment. The authors thank the donors of the Petroleum Research Fund, administered by The American Chemical Society (41009-AC7), the National Science Foundation (DMR 9986123, DGE 9972776), and the TouchSensor Technologies LLC. for support of the research. We are grateful to Prof. A. Matzger for use of the polarizing microscope and the powder pattern indexing programs, to Dr. Larry Beck for obtaining the SS-NMR spectra, and to Prof. O. Yaghi for use of the variable-temperature powder diffractometer.

Supporting Information Available: Experimental section, including syntheses and measurement methods, Figures S-1 to S-20, and Tables S1 to S3. This material is available free of charge via the Internet at http://pubs.acs.org.

JA076235T

(68) Bolognesi, A.; Porzio, W.; Bajo, G.; Zannoni, G.; Fannig, L. *Acta. Polym.* **1999**, *50*, 151−155.
(69) Park, K. C.; Levon, K. *Macromolecules* **1997**, *30*, 3175−3183.
(70) Neue, G.; Dybowski, C. *Solid State Nucl. Magn. Reson.* **1997**, *7*, 333.